Production Engineering (2024) 18:339–351
https://doi.org/10.1007/s11740-023-01247-x

PROCESSES

Towards developing a control of grinding processes using a combination of grinding power evaluation and Barkhausen noise analysis

Rahel Jedamski[1] · Gerrit Kuhlmann[1,2] · Maximilian Rößler[3] · Bernhard Karpuschewski[1,2,4] · Martin Dix[3] · Jérémy Epp[1,4]

Received: 31 August 2023 / Accepted: 23 November 2023 / Published online: 2 January 2024
© The Author(s) 2023

Abstract
After grinding of hardened workpieces, especially in case of safety-relevant components, usually non-destructive testing is carried out to detect thermo-mechanical damages in the surface layer. In-process detection methods allow a fast reaction to negative changes before producing a large amount of rejects and open the possibility to save additional time for post-process inspection. However, these are not industrially used yet, since boundary conditions and application limits are not defined so far. This study shows the potential of a grinding process control based on a soft sensor combining a thermal limit in a $P_c''-\Delta t$-diagram and magnetic Barkhausen noise analysis applied in-situ during grinding (BN). The specific grinding power P_c'' in dependence of the contact time Δt allows to identify/avoid grinding burn starting from light tempering zones. Furthermore, the BN is well suited for the detection of detrimental residual stress changes (tensile) occurring even before tempering zones are generated. The developed process control based on this combination optimizes the process parameters to prevent negative thermo-mechanical surface changes while keeping the productivity of the process as high as possible. The applicability is demonstrated for external cylindrical and non-circular grinding processes. Due to the radius varying over the workpiece circumference, the latter ones require special demands on signal evaluation, resolution and control speed.

Keywords Grinding · Surface integrity · Grinding burn limit · Process control · Barkhausen noise

1 Introduction

Grinding of hardened components bears the risk of thermo-mechanical surface damages and therefore requires a reliable method for the detection of damages [1]. Due to the high frictional energy in the contact zone between grinding wheel and workpiece, heat is generated and can lead to a deterioration of surface properties. These negative changes can include the shift of residual stresses into tensile direction, tempering zones with decreased hardness, rehardening and micro cracks [2].

Different from laboratory methods like X-ray diffraction or metallographic analysis, non-destructive detection methods like nital etching or Barkhausen noise (BN) analysis allow a 100% testing of manufactured parts [2]. However, in case of nital etching, this advantage is contrasted by high time effort, subjectivity and environmental risks [1].

1.1 Barkhausen noise

The magnetic BN is based on the cyclic magnetization of a ferromagnetic material volume consisting of unidirectional magnetized areas separated by Bloch walls. Under the influence of an external magnetic field the magnetization takes place due to growth of favorably oriented domains, shift of Bloch walls and rotation of the magnetic domains [3]. This stepwise movement of Bloch walls is detectable

✉ Rahel Jedamski
jedamski@iwt-bremen.de

1 Leibniz Institute for Materials Engineering—IWT, Bremen, Germany

2 University of Bremen, Chair of Machining Technologies, Bremen, Germany

3 Fraunhofer Institute for Machine Tools and Forming Technology IWU, Chemnitz, Germany

4 MAPEX Center for Materials and Processes, University of Bremen, Bremen, Germany

as Barkhausen noise [4] and sensitive to changes in microstructure and residual stresses [5].

Therefore, it is well suited for the detection of thermo-mechanical surface changes [1] including changes of the residual stress state occurring before microstructural changes referred to as tempering zones with a decrease of hardness [2]. On the other hand, an unambiguous detection and distinction of all surface states is not always possible with only one measurement parameter. After an increase of the BN level with tensile residual stresses and the occurrence of light tempering the Barkhausen amplitude decreases with heavier tempering and rehardening, which requires specific strategies like the combination with other characteristic values from BN [6, 7] or another method [8].

In addition to the established post-process measurements some approaches for in-process measurement of BN during grinding are currently being developed. First trials on the in-process use of BN were already conducted around the year 2000 [9] [10]. Questions about lifetime of the sensors in the harsh environment of grinding machines and wear of sensor and workpiece thereby remained open. Newer approaches use coated sensors [11] or contactless measurements [12] to avoid wear. They are not industrially used yet, but promise the possibility of an early reaction to beginning negative changes [11, 12]. Especially for non-circular grinding processes only single investigations exist [13].

1.2 Process model—P_c''– Δt-diagram

Possible other methods for the monitoring of grinding processes are analytical approaches like the grinding burn limit developed by Malkin [14] based on the thermal model from Carslaw and Jaeger [15]. Further models like surface layer modification charts with maximum surface zone temperature and contact time [16] or the relationship of chip thickness, specific grinding energy and thermal damages [15] combine analytical knowledge with empirical data. Application of this models requires complex tools like grinding wheels with integrated temperature measurement system [16].

In [8, 17] and [18] the suitability of surface layer modification charts containing the specific grinding power P_c'' and the contact time Δt for the non-destructive grinding burn detection was shown. Based on the work of Malkin [19] a lower limit for the occurrence of grinding burn, visible in metallographic micrographs could be identified [17]. The specific grinding power P_c'' is calculated according to Eq. 1, where P_c is the grinding power, a_p the grinding width, l_g the contact length between grinding wheel and workpiece, F_t the tangential force and v_c the cutting speed. The contact time Δt is calculated from l_g and the tangential feed speed v_{ft} (Eq. 2). From Malkin´s experimental data for flat and external cylindrical grinding processes the grinding burn limit was calculated as $P_c'' = 7.1 \bullet \Delta t^{-0.523}$ with a correlation coefficient of $R^2 = 0.96$, using the tangential grinding force for calculation of P_c'' [20].

$$P_c'' = \frac{P_c}{a_p \bullet l_g} = \frac{F_t \bullet v_c}{a_p \bullet l_g} \tag{1}$$

$$\Delta t = \frac{l_g}{v_{ft}} \tag{2}$$

This limit was also verified for grinding processes with shorter (continuous generating gear grinding) and longer (discontinuous profile grinding [18]) contact times and different case hardening steel grades [17]. Furthermore, the process model was applied for a non-circular grinding process. This requires a locally resolved calculation of contact lengths and times [13]. It is to mention that the thermal limit according to Malkin is an indicator for the occurrence of tempering zones [19], beginning changes of the surface state cannot detected.

1.3 Soft sensors

Combinations of physical measurement principles (e.g. micromagnetic methods, temperature or acoustic emission measurements [21]) with other information (e.g. model-based knowledge, FE simulation [21]), using a mathematical model are referred to as soft sensor [21]. Soft sensors can be model-based or data-driven and deliver information about e.g. product properties in real time [23]. They are able to generate information not achievable with only physical sensors and are therefore well suited for the monitoring of surface integrity during machining as an element of process control [21, 22].

Most soft sensor approaches for the monitoring of surface integrity are based on complex models requiring an individual calibration with a large number of measurements. Also, simulations are often used [21]. While these individual calibration for e.g. different materials implies a high time effort the validity of the P_c''– Δt-diagram was demonstrated for various steel grades and grinding processes [17].

1.4 Conceptualization

Aim of this study is to show the potential of a soft sensor combining in-process BN measurements and a surface layer modification chart based on specific grinding power and contact time (process model) for the control of grinding processes. While tempering and rehardening zones can be excluded by the process model, the BN is particularly sensitive to slight changes of the surface state. The combination

of both methods is expected to unambiguously detect all grades of surface changes. The suitability of the physical (BN) sensor as well as the process model is shown and the need to combine both is demonstrated for cylindrical (chapter 3.1) and non-circular (chapter 3.2) grinding process kinematics. The results are validated by metallographic analyses and residual stress depth profiles. Finally, a concept for the realization of a grinding process control is presented (chapter 3.4).

2 Material and methods

Investigations were performed during cylindrical and non-circular grinding of workpieces from AISI 4820 respectively AISI 52100. BN analysis was carried out with two different measurement systems. In the following the grinding processes and measurement setups are described.

Table 1 Process parameters for cylindrical grinding

Cutting speed v_c	35 m/s
Speed ratio q	90
Radial feed speed v_{fr}	0.28/1.69/2.82 mm/min
Specific material removal rate Q'_w	1/6/10 $mm^3/(mm{\cdot}s)$
Total depth of cut a_e	100 µm
Metal working fluid flow rate Q_{MWF}	40 l/min
Overlap ratio dressing U_d	3 (form roller)
Speed ratio dressing q_d	− 1
Depth of dressing a_{ed}	2 × 20 µm

After grinding, the generated surface states were characterized by residual stress depth profiles, metallographic analyses and hardness measurements. Residual stress measurements were performed at α{211} peak with a diffractometer type MZ IV (GE Inspection Technology, Ahrensburg, Germany) with Cr-Kα-radiation and a beam diameter of 2 mm using the $\sin^2\psi$ method. The micrographs were etched with a 3% alcoholic HNO_3 solution and investigated with an optical microscope Zeiss Axiophot (Carl Zeiss AG, Oberkochen, Germany). Surface hardness according to Vickers was measured with a LV-700AT (LECO Instrumente, Mönchengladbach, Germany).

2.1 Setup of the cylindrical grinding process

A cylindrical outer diameter grinding process was carried out on a grinding machine Studer S41 (Fritz Studer AG, Steffisburg, Switzerland). Case-hardened cylindrical workpieces from AISI 4820 (Ø67.7 mm × 152 mm, surface hardness 665 ± 17 HV1, case hardening depth 1.76 mm) were machined with a corundum grinding wheel 54A120 H15VP-MF904W (500 mm × 36 mm × 203.2 mm) and the process parameters given in Table 1. As metal working fluid oil of the type Rhenus EG 10 was used. BN was measured with a 3MA-II device (Fraunhofer IZFP, Saarbrücken, Germany) and a special sensor for in-process use. The sensor was fixed in an isolating holder. An adjustable spacer and a spring ensured a constant air gap of 200 µm between sensor and workpiece surface. Interfering signals were eliminated by an isolating transformer and a potential equalization between housing of the 3MA-II device and tailstock of the grinding machine. The setup is shown in Fig. 1. Further details are

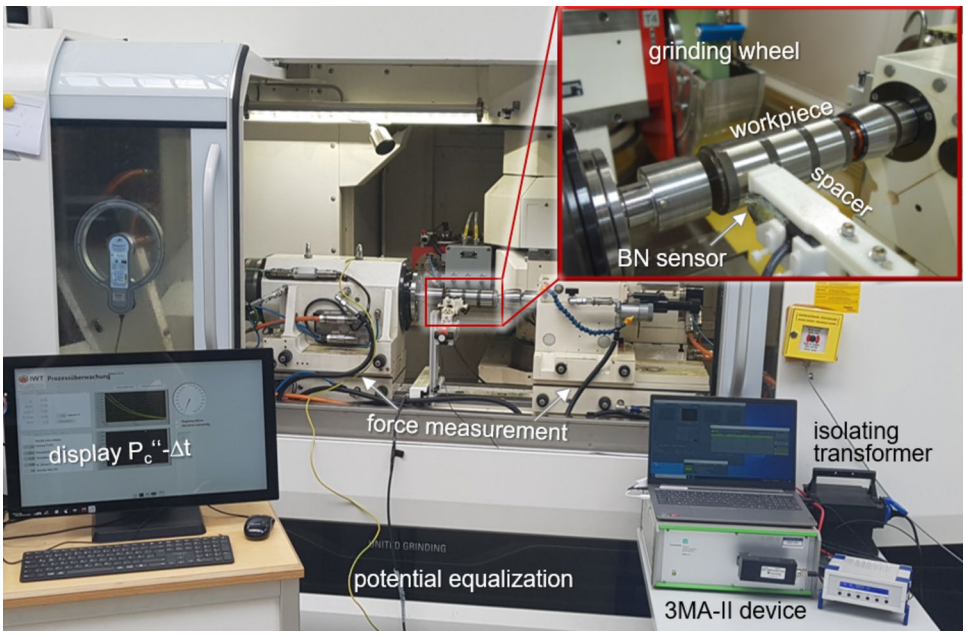

Fig. 1 Setup of the cylindrical grinding process

described in [12]. This study also demonstrates the applicability of BN for in-process monitoring despite the rough conditions and interfering influences in the grinding machine. BN measurements were carried out with a magnetization frequency of 120 Hz, a magnetization amplitude of 100 A/cm and an analyzing frequency range from 100 to 1000 kHz. Process forces (tangential force F_t, normal force F_n) were measured by a piezoelectric measurement system integrated in workpiece spindle and tailstock and the effective power of the grinding spindle was recorded.

2.2 Setup of the non-circular grinding process

The non-circular grinding process was performed on a universal outer diameter grinding machine Kelvaria UR175-1500 (Kellenberger, St. Gallen, Switzerland) with a corundum grinding wheel 3SK3 80H12 VEG (100 mm × 20 mm). The workpiece is an induction hardened cam from AISI 52100 (56 + 5 HRC, surface hardening depth 1.3 mm, base diameter 33.4 mm, cam height 2.025 mm), the metal working fluid an emulsion with the water mixable half-synthetic coolant B-Cool 9665. The grinding parameters are given in Table 2. Prior to the actual grinding process the cams were ground with a radial feed speed of $v_{fr} = 0.06$ mm/min which is used for finishing in industry. Due to the cam geometry Q'_w varies over the circumference. The given maximum is reached on the concave flanks.

BN measurements were carried out with a Rollscan 300 (Stresstech GmbH, Rennerod, Germany) with magnetization frequency 125 Hz, magnetization voltage 16 V and analyzing frequency range 70 to 200 kHz. A constant gap of 100 µm between workpiece and sensor is realized by a plastic foil covering the surface of the sensor. The setup of the sensor in the grinding machine is shown in Fig. 2. In addition to the mp value, the raw signal of the BN, the effective power of the grinding spindle and the position of the workpiece's axis of rotation were recorded using a

Table 2 Process parameters for non-circular grinding

Cutting speed v_c	35 m/s
Rotational speed workpiece n_w	26.8 min^{-1} – 28.2 min^{-1}
Radial feed speed v_{fr}	0.06/0.36/1.2 mm/min
Max. spec. mat. removal rate Q'_w	0.4/2.3/7.6 $mm^3/(mm{\cdot}s)$
Total depth of cut a_e	10/60/200 µm
Fluid flow rate Q_{MWF}	20 l/min
Overlap ratio dressing U_d	3 (stationary dresser)
Depth of dressing a_{ed}	5 × 10 µm

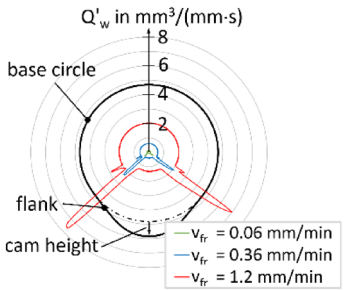

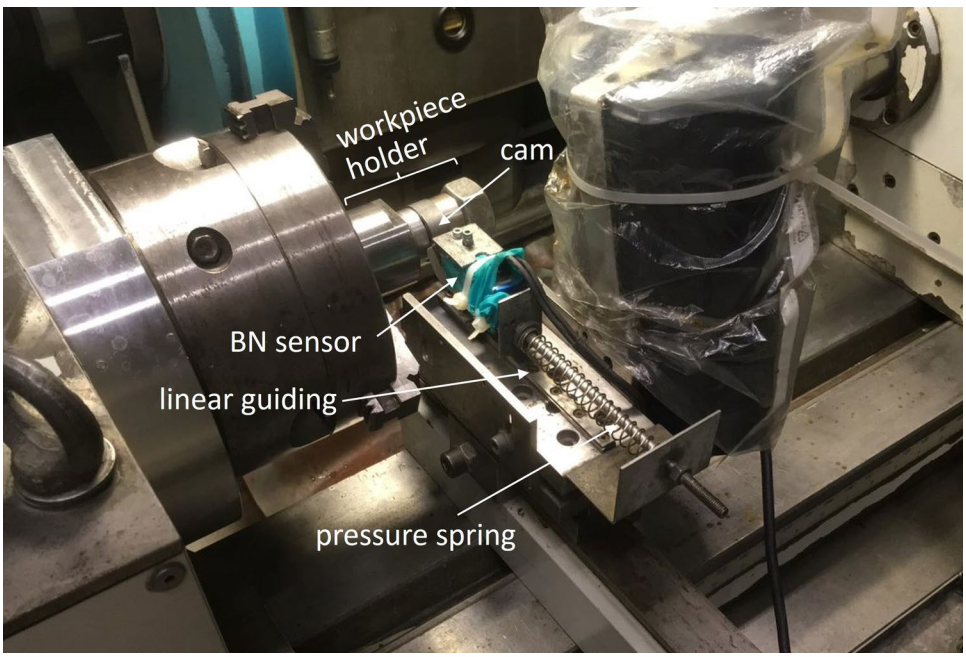

Fig. 2 Setup of the non-circular grinding process

transient recorder LTT24 (Labortechnik Tasler, Würzburg, Germany).

3 Results and discussion

In the following, the combined use of the P_c''-Δt-diagram and BN measurements as a soft sensor for the detection of thermo-mechanical surface changes during grinding is demonstrated for the cylindrical and the non-circular grinding process and validated by destructive characterization. Afterwards, approaches for a control system based on this soft sensor are described.

3.1 Cylindrical grinding process

Figure 3 shows the specific grinding power P_c'' during cylindrical grinding processes with different specific material removal rates as well as the grinding burn limits according to the equations given in chapter 1 for the different processes. For better overview the time axis is given as a percentage of the machining time from beginning of the grinding wheel contact to the beginning of sparking out. Besides calculating the power from the tangential force like in previous works [8, 20] also the spindle power was considered for the calculation of P_c'' (Eq. 1). Additionally, the corrected spindle power was calculated by subtracting the machine base load, as illustrated in Fig. 3c). Despite the correction, a difference $\Delta P_c''$ (Fig. 3b)) between P_c'' calculated from the corrected spindle power and tangential force exists and will be discussed later. The limit values for the occurrence of grinding burn depend on the contact time, which is constant during a certain grinding process. P_c'' and Δt are calculated according to (1) and (2). The geometrical contact length l_g for cylindrical grinding processes is given in (3). f_r is the radial feed (per rotation), d_w the workpiece diameter and d_c the grinding wheel diameter [24].

$$l_g = \sqrt{f_r \frac{d_w \bullet d_c}{d_w + d_c}} \tag{3}$$

During grinding with $Q'_w = 10$ mm³/(mm·s) P_c'', calculated from the tangential force as well as from the corrected spindle power, exceeded the grinding burn limit (Fig. 3a)). The metallographic micrograph and hardness measurements (Fig. 4a)) confirm the existence of a beginning tempering zone. Therefore, the specific material removal rate for the next workpiece was reduced to 6 mm³/(mm·s) and the maximum P_c'' calculated from the tangential force decreased to

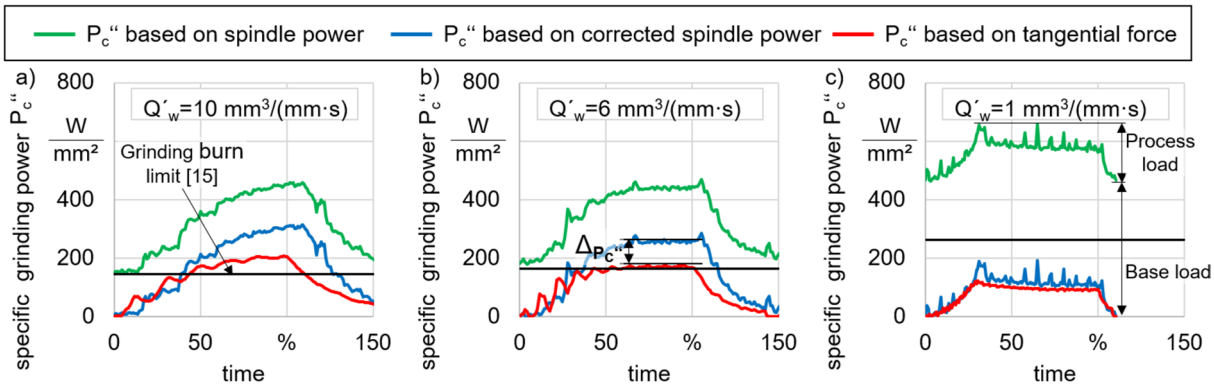

Fig. 3 Specific grinding power P_c'' during grinding processes with specific material removal rates Q'_w of 10 mm³/(mm·s) (**a**), 6 mm³/(mm·s) (**b**) and 1 mm.³/(mm·s) (**c**)

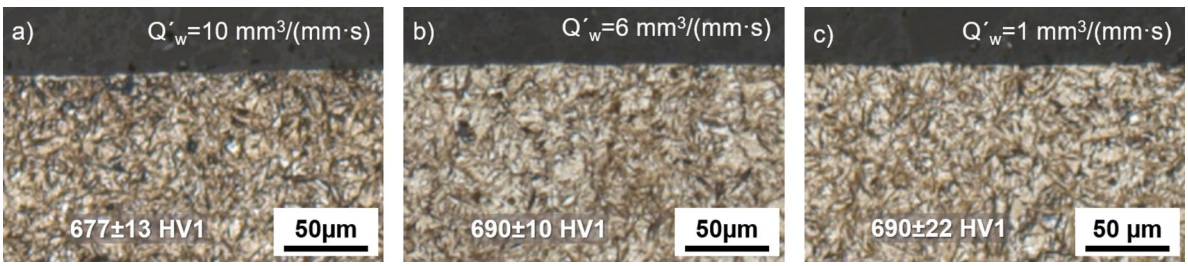

Fig. 4 Metallographic micrographs of samples ground with specific material removal rates of 10 mm³/(mm·s) (**a**), 6 mm³/(mm·s) (**b**) and 1 mm.³/(mm·s) (**c**)

a value around the grinding burn limit. Hence, a tempering zone cannot be completely excluded. A grinding burn evaluation based on the corrected spindle power would lead to the result that grinding burn has occurred. The metallographic micrograph and the surface hardness (Fig. 4b)), however, show that no tempering zone was generated.

The results show that the already verified force-based approach cannot be completely transferred to P_c'' calculated from the corrected grinding power. Nevertheless, in industry-related concepts there is an interest in using the corrected grinding power instead of calculating from tangential force because of the less precise but more simple measurement. To take the non- constant difference $\Delta P_c''$ into account, a compensation function is determined from the data shown in Fig. 3 and further processes with other specific material removal rates under the same conditions. $\Delta P_c''$ increases with higher Q'_w. As a first approximation the linear function with a correlation coefficient of $R^2 = 0.94$ shows a good correlation (Fig. 5) but further trials are recommended for improvement. Existing studies show that e.g. cooling lubricant supply conditions like different nozzle types, nozzle positions or flow rates and process parameters like cutting speed influence the process power [25]. Therefore, compensation functions have to be determined for each grinding process and are limited for these parameters.

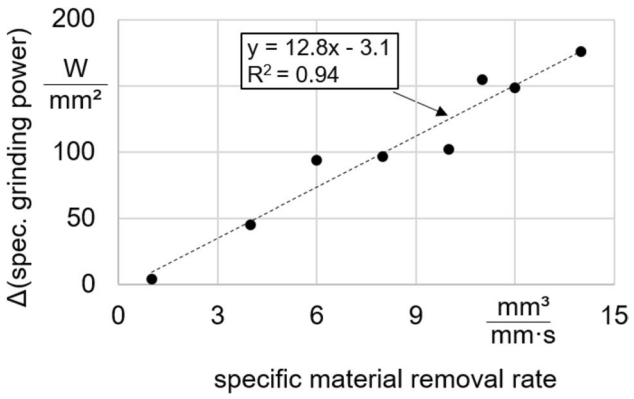

Fig. 5 Correction function for consideration of $\Delta_{Pc''}$

Although visible tempering zones can be excluded, negative changes of the residual stress state can already occur before. Therefore, in the following, the in-process measured BN values are considered additionally. Figure 6 shows the evolution of the maximum BN amplitude M_{MAX} (blue dots) during grinding processes with different specific material removal rates. In addition, the course of the tangential force F_t (red line) and a limit value for M_{MAX} (blue line) are shown. The limit value for critical residual stress states has to be defined based on preliminary investigations for the respective workpiece geometry, steel grade and heat treatment. In this case, two grinding processes without negative influence on the surface state were considered and the maximum plus standard deviation ($M_{MAX} = 0.147$ V) was chosen as limit value (blue line). Besides M_{MAX}, the 3MA-II method provides further parameters from the BN envelope whose suitability are discussed in [26].

At the beginning of all grinding processes M_{MAX} was at a high and scattering level around 0.2 V because of the soft surface oxidation layer from gas carburization. Pre-grinding for the removal of this layer wasn´t performed. During grinding with $Q'_w = 10$ mm³/(mm·s) (Fig. 6a)) M_{MAX} stayed at a high level due to the tempering zone also detected based on P_c''. For $Q'_w = 6$ mm³/(mm·s) M_{MAX} decreased with beginning of the grinding wheel contact (visible in the increase of F_t) due to the removal of the soft layer but stayed clearly over the limit value (Fig. 6b)). Therefore, it can be assumed that lower compressive or even tensile residual stresses are present, what is confirmed by the residual stress profiles. Figure 7b) shows that the axial residual stresses in a depth of 10 to 20 µm

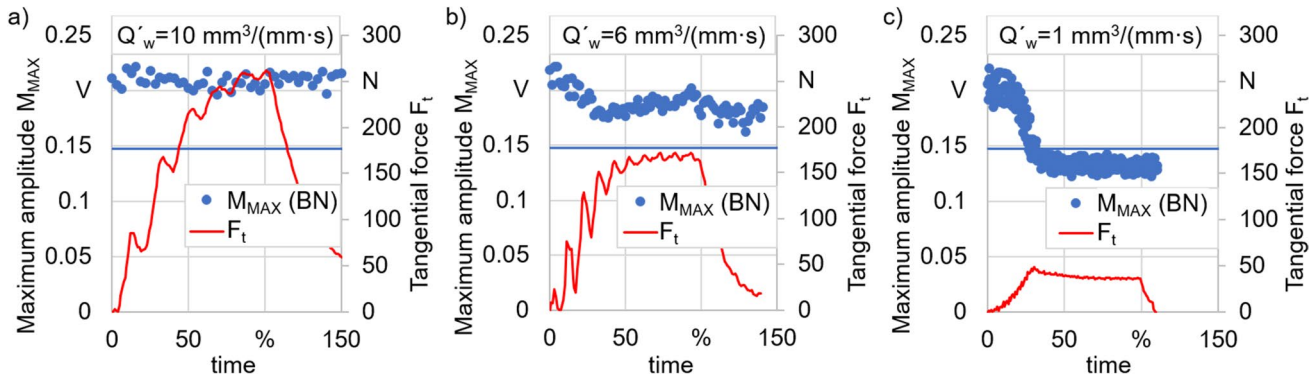

Fig. 6 Maximum BN amplitude and tangential force during grinding processes with specific material removal rates Q'_w of 10 mm³/(mm·s) (**a**), 6 mm³/(mm·s) (**b**) and 1 mm³/(mm·s) (**c**) as a function of relative grinding process duration

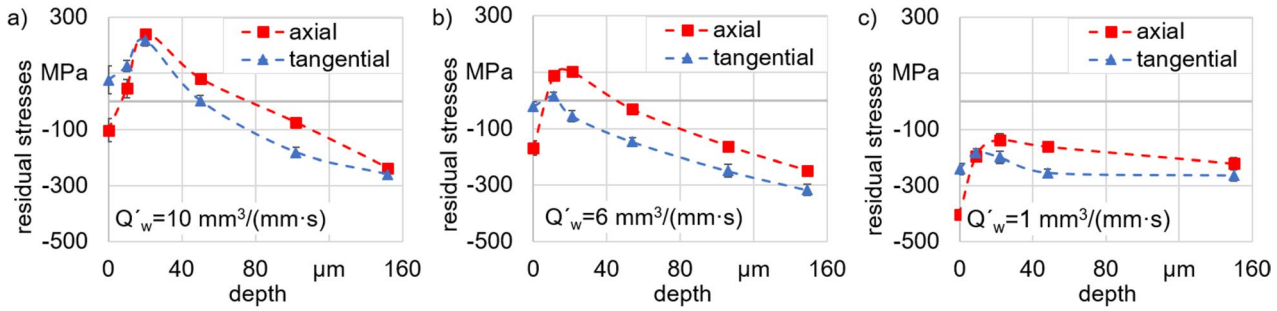

Fig. 7 Residual stress depth profiles of samples ground with specific material removal rates of 10 $mm^3/(mm{\cdot}s)$ (**a**), 6 $mm^3/(mm{\cdot}s)$ (**b**) and 1 $mm.^3/(mm{\cdot}s)$ (**c**)

are around 100 MPa and in tangential direction the maximum is slightly in the tensile range. At the surface the mechanical influence from grinding leads to compressive residual stresses while in larger depths the thermal influence dominates [27]. The mechanical effect is intensified by sparking out at the end of the grinding process. High compressive residual stresses have a positive influence on components lifetime [27]. Consequently, the next workpiece was ground with lower specific material removal rate of $Q´_w = 1\ mm^3/(mm{\cdot}s)$. As expected, neither Fig. 3 c) nor Fig. 4 c) indicate tempering zones and also M_{MAX} is below the limit for critical (tensile) residual stress states. Figure 7c) confirms that the residual stresses are completely in the compressive range with − 100 to − 300 MPa. For the used grinding parameters with a maximum $Q´_w$ of 10 $mm^3/(mm{\cdot}s)$ M_{MAX} always rises with increasing thermo-mechanical surface changes. The decrease of M_{MAX} with higher thermo-mechanical impact is shown in [26] and would strongly require the combination with the P''_c – Δt-diagram.

For demonstration reasons, in this example larger steps between the specific material removal rates were chosen. In grinding process control, finer adjustment steps would allow defining optimal productivity without the risk of negative thermo-mechanical surface changes. By choosing the limit value for M_{MAX} it is also possible to define up to which point beginning changes of the residual stress state are still tolerated.

3.2 Non-circular grinding process

Due to the varying radius and rotational speed of the cam, the application of the grinding burn limit to non-circular grinding processes requires an angle-resolved calculation of P''_c, Δt and the thermal limit. Figure 8 shows the specific grinding power together with the grinding burn limit in dependence of the process time for grinding processes with different radial feed speed. The workpiece velocity v_w is calculated from the coordinates of the C axis (workpiece axis), l_g is the result of a two-dimensional simulation [13]. The different areas of the circumference are marked in blue (flanks and tips) and red (base circle). As to be expected regarding Q'_w, the highest P''_c appeared in the area of the flanks. Although even the grinding burn limit is higher in

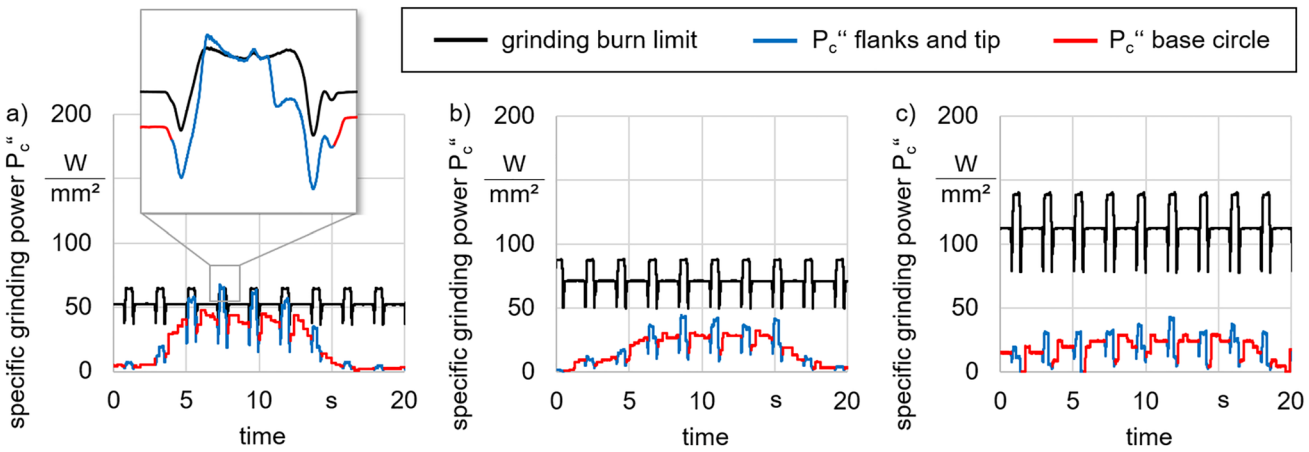

Fig. 8 Specific grinding power P''_c during grinding processes with radial feed speed of 1.2 mm/min (**a**), 0.36 mm/min (**b**) and 0.06 mm/min (**c**)

this area, it was slightly exceeded during grinding with $v_{fr} = 1.2$ mm/min. Thus, tempering zones are to be expected and the radial feed speed has been reduced to 0.36 mm/min for the next cam.

The residual stresses in direction of grinding and the full width at half maximum of the X-ray peak (FWHM) were measured at the tip (0°), the flank (40°) and the base circle (130°) of the ground cams. Figure 9a) confirms the presence of a tempering zone on the flank ground with $v_{fr} = 1.2$ mm/min. The maximum residual stresses are almost 800 MPa instead of compressive range or around 0 MPa. Further, the FWHM which is influenced by the microstructure [28] and correlates with the hardness after grinding [7, 29], is reduced. A smaller difference exists between surface states at the tip and on the base circle where residual stresses are slightly more in the tensile range.

During grinding with $v_{fr} = 0.36$ mm/min P_c'' was under the grinding burn limit for the complete circumference of the cam and even Fig. 9b) indicates no tempering zone. To exclude critical residual stress states without a hardness drop, the in-process measured BN was considered as well. As already observed in [30] especially for light workpieces, in-process BN measurements are affected by the mechanical excitation of Bloch wall movements caused by the

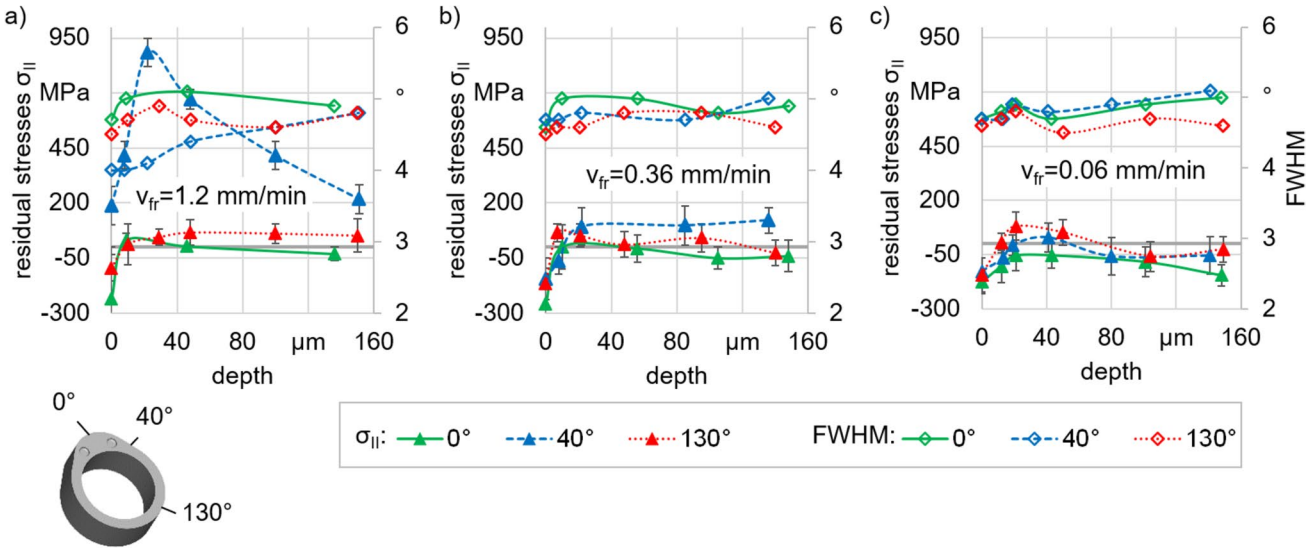

Fig. 9 Residual stress and FWHM depth profiles of cams ground with radial feed speed of 1.2 mm/min (**a**), 0.36 mm/min (**b**) and 0.06 mm/min (**c**)

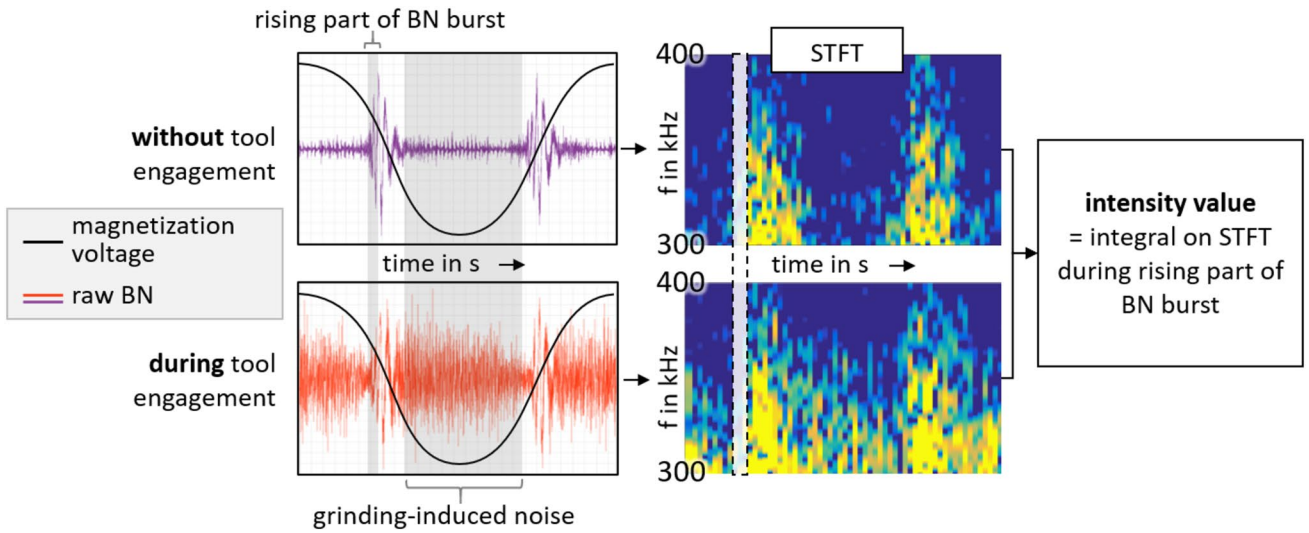

Fig. 10 Data treatment approach for elimination of grinding-induced noise

engagement of the grinding wheel. As shown in Fig. 10, this excitation leads to an increased BN at the maximum magnitude of the magnetization voltage. Consequently, there is a significant increase in the mp value calculated as the root mean square value of the BN over one magnetization cycle. An in-process detection of residual stress changes is not possible using this parameter.

To eliminate the grinding-induced noise, the recorded raw BN signal is split into its single magnetization cycles. Then, a Short-Time Fourier Transformation (STFT) is used to transform the signal parts into the time–frequency domain. In the STFT, during the rising flank of the BN burst, there is a band between 300 and 400 kHz which is (almost) unaffected by the grinding process. Integrating over this band, a value for the intensity of the BN is calculated.

Another challenge for BN measurements on non-circular workpieces are the not constant contact conditions [13]. As shown in Fig. 11, the BN-sensor contacts the cam's flanks off-center. In contrast, the contact at the base circle and at the tip is centric. As a result, the size of the air gap between BN sensor and cam varies and therefore the height of the BN is influenced, regardless of the residual stress state [31]. To eliminate the influence of the contact conditions of the sensor, a references BN value is assigned to the respective position of the cam's circumference by a pre-process measurement after pre-grinding with finishing speed $v_{fr} = 0.06$ mm/min (Fig. 11 b)). For subsequent measurements, the recorded value is divided by the reference value. A ratio unequal to 1 (ignoring the noise character of the signal) indicates changes compared to the reference state. Longer term, a smaller sensor tip could help to minimize the influence of the contact conditions.

Grinding with a radial feed speed of $v_{fr} = 1.2$ mm/min led to an increased intensity value for the entire cam's circumference (Fig. 12a)). The most significant increase was at the flanks, recognizable by two signal peaks per cam revolution.

Reducing the radial feed speed to $v_{fr} = 0.36$ mm/min, the intensity value still increased slightly during the grinding

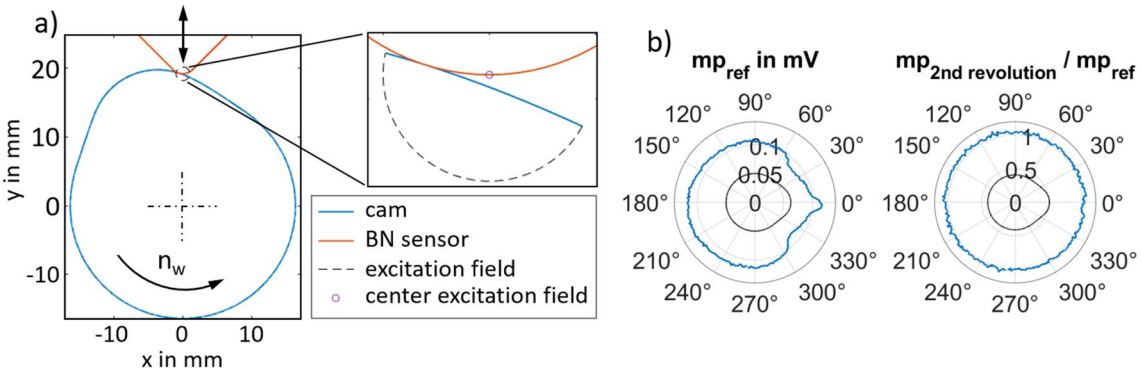

Fig. 11 Schematical view of the contact between BN sensor and cam during one revolution [13] (**a**), Elimination of the geometric influence using reference data (**b**)

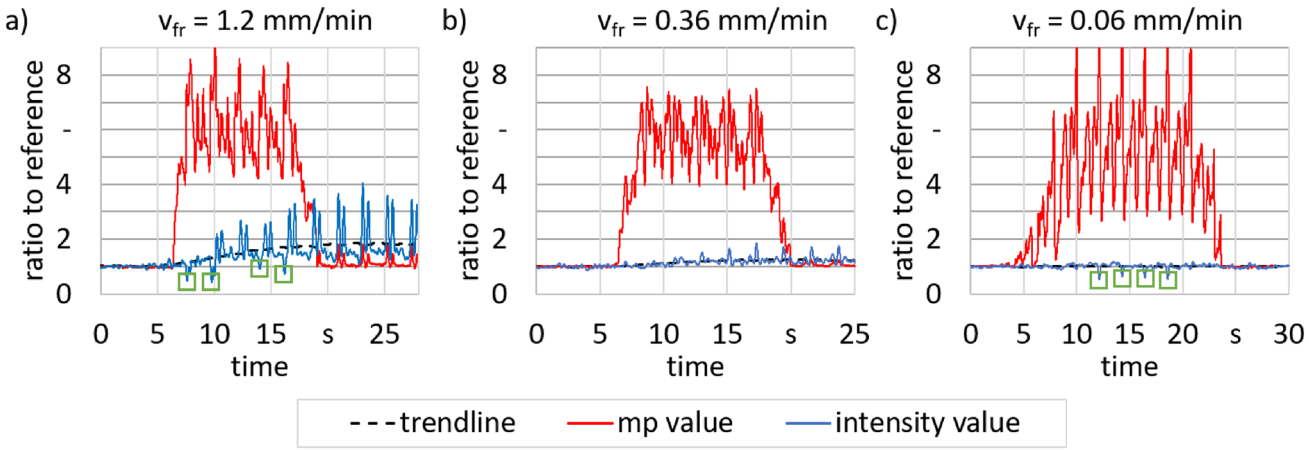

Fig. 12 Intensity and mp value of the BN during grinding processes with radial feed speed of 1.2 mm/min (**a**), 0.36 mm/min (**b**) and 0.06 mm/min (c) as ratio to a reference

process and reached the highest values at the flanks. The residual stress changes indicated by the intensity value are confirmed by the residual stress profiles (Fig. 9). As shown in Fig. 9b), the residual stresses on the flank are higher than the values at the base circle and the tip. Furthermore, the flank's residual stresses remained positive from a depth of 20 µm.

Therefore, the finishing feed speed of $v_{fr} = 0.06$ mm/min used in series production was applied in a third trial. Both the intensity value and the residual stresses staying around or below 0 MPa in Fig. 9c) indicated a surface state corresponding to the accepted finishing state.

The reason for the signal dips marked in Fig. 12a) und c) (green) is not a shift of residual stresses, as shown by the post-process signal behavior of mp and intensity value, but the described calculation principle used to eliminate the grinding-induced noise.

3.3 Summary of experimental results

Figure 13 gives an overview of the correlation between the measured respectively calculated parameters (BN values, P_c'') and the monitored surface states for the cylindrical and the non-circular grinding process. The plotted values (P_c'', BN values) are the maximum of the respective process, during non-circular grinding this maximum appears always on the cam flanks. The contact time Δt and thus the grinding burn limit differs between cylindrical and non-circular grinding and between the different Q'_w respectively v_{fr}. But for all grinding processes, grinding burn visible in the metallographic micrograph, is also indicated by a P_c'' over the grinding burn limit. b) and c) show the correlation between residual stress state and BN values. A direct comparison of cylindrical and non-circular grinding processes is not possible because of the different measurement (and calculation) methods and steel grades. Nevertheless, both graphs show a non-linear increase of the BN signals with shift of the residual stresses into tensile direction.

3.4 Grinding process control

Figure 14 shows an approach for a grinding process control based on the combination of the evaluation of the specific grinding power and the BN. Figure 14a) gives an overview over the closed-loop control according to [22]. The result of the grinding process is influenced by the manipulated variable, in the example the radial feed speed v_{fr}, and disturbance variables like the grinding wheel condition or differences in the workpiece geometry. Controlled variable is the surface state after respectively during grinding characterized by residual stresses and hardness. These properties cannot be measured during the grinding process but determined by a soft sensor. For this purpose, in-process measured grinding power and BN are acquired as analogue signals (voltage). In case of the 3MA-II measurement technology an additional software module is used to provide measurement results as analogous signal in real-time. Figure 14b) shows the soft sensor in detail. As first criterion the specific grinding power is compared with the grinding burn limit in the P_c''-Δt diagram. Besides the current grinding power, this requires additional information like the workpiece and grinding wheel diameter or the rotational speed of the workpiece. If the specific grinding power is higher than the limit value, the

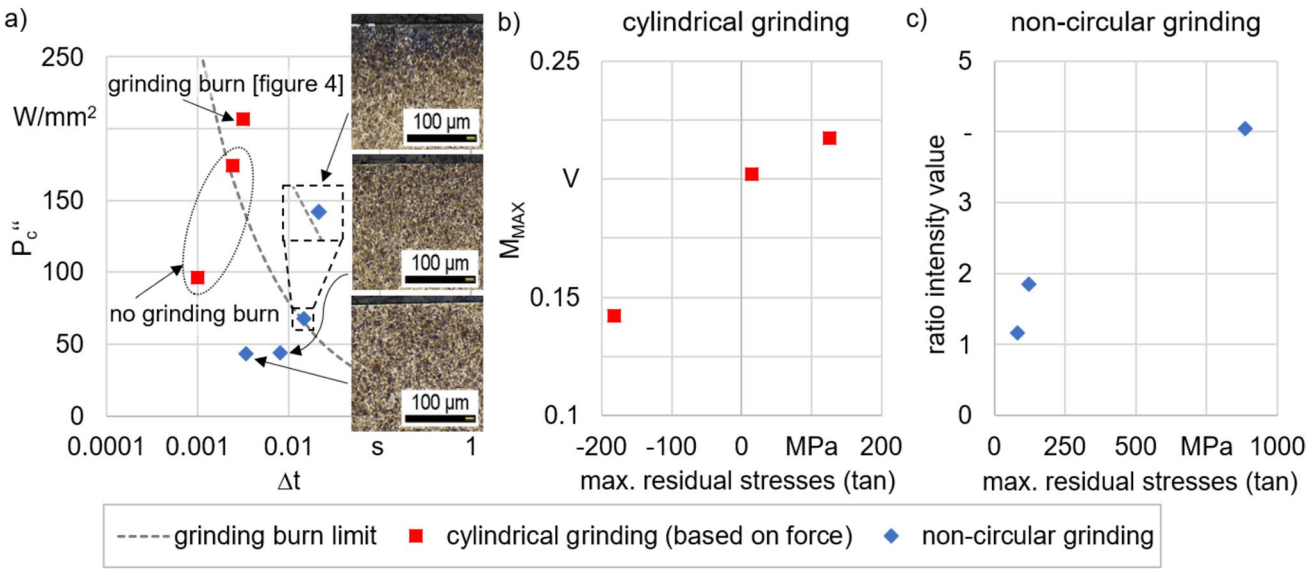

Fig. 13 Overview of the experimental points in P_c''-Δt-diagram (**a**) and correlation between BN values and residual stress state (**b**, **c**)

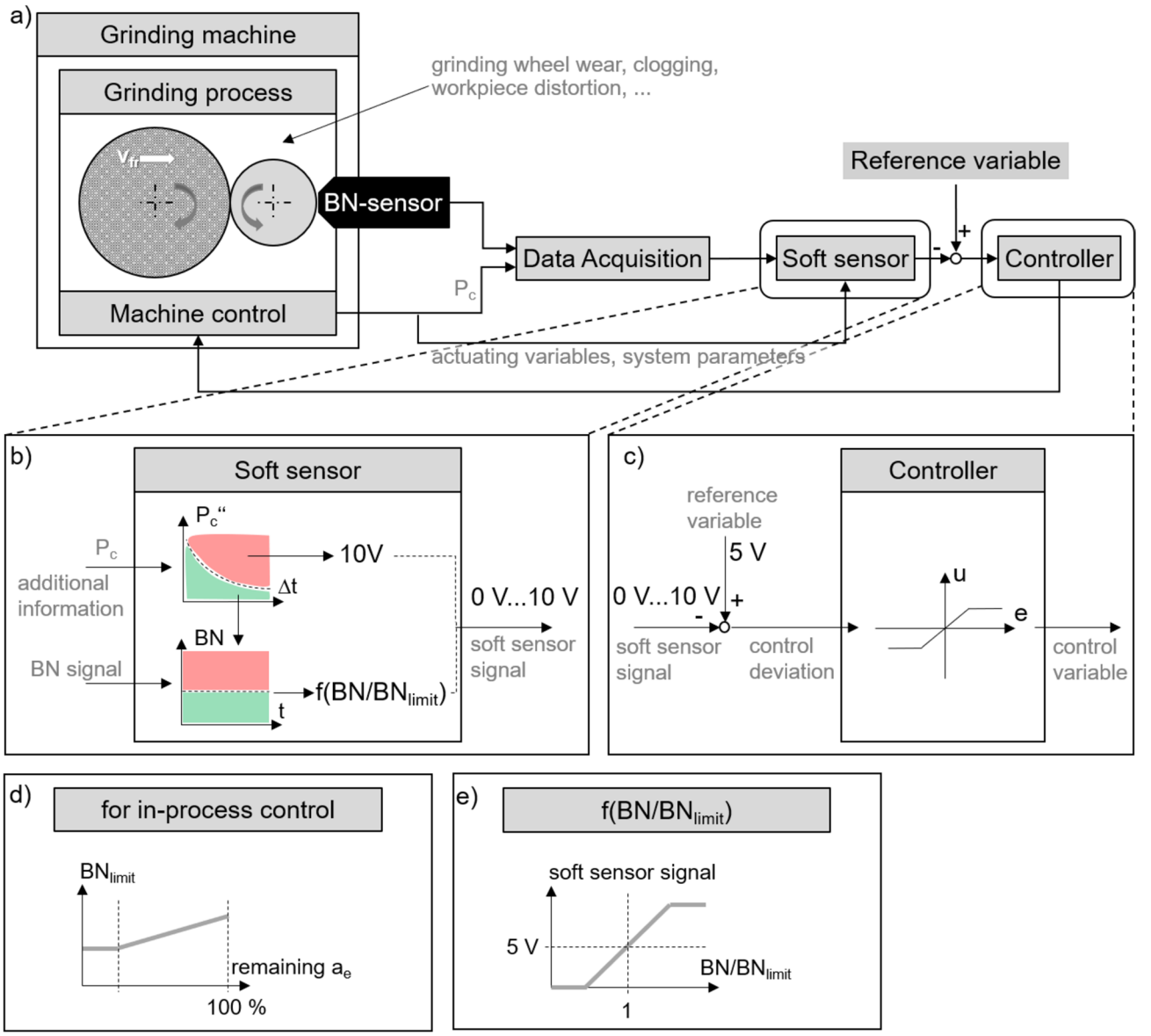

Fig. 14 Schematic view of the planned grinding process control (**a**) with soft sensor (**b**, **d**, **e**) and controller (**c**)

workpiece is considered as damaged and the maximum soft sensor signal of 10 V is given out. Otherwise, the second criterion, the level of the BN signal, is applied by comparing the BN (as analogous signal) with a defined limit value. The soft sensor signal is calculated from the ratio of the measured BN and BN_{limit} (Fig. 14e).

The controlled variable determined this way (soft sensor signal as voltage) is compared with the defined reference variable (Fig. 14c). From the control deviation e, a controller determines an analogous voltage signal between 2.5 and 7.5 V which overrides the software potentiometer of the machine tool control and thus adjusts the override for v_{fr} between 50 and 150%. In [32] the functionality of this principle was confirmed for the control of the feed rate on the basis of an effective power signal.

For external cylindrical grinding, in general the surface state is constant over the workpiece circumference. The control can be performed from one workpiece to the next, thus a rather slow PID controller is sufficient. For non-circular grinding, thermo-mechanical damage of the surface state occurs locally on the circumference due to the curvature—e.g. on the concave flanks regarding cam grinding. Therefore, the control is realized in-process. For implementation, the workpiece contour is divided into a defined number of ring buffer segments [13]. A controller is assigned to the respective segment using the principle shown in Fig. 14. This requires a faster controller,

probably a cascade controller, that will be developed in future work.

In the case of a control from one workpiece to the next, a workpiece with a soft sensor signal over the reference variable always has to be rejected. For an in-process control it depends on the remaining stock a_e whether a surface damage can be corrected or the part also has to be rejected. For further optimization of the productivity it could be an option to allow a higher BN_{limit} and thus a higher feed speed at the beginning of a grinding process than for finishing at the end (Fig. 14d).

Instead of the manipulated variables, also an optimization of the dressing intervals is possible by using the soft sensor. Due to wear and clogging and thus increasing thermal load, dressing of the grinding wheel has a large impact on the surface state. A control allows time and cost savings by maximization of the grinding wheel lifetime without risking thermo-mechanical surface damages.

4 Conclusions

The present study shows how a soft sensor combining a thermal limit based on the grinding power and in-process measurements of the magnetic Barkhausen noise can help to avoid thermo-mechanical surface damages and increase the productivity of grinding processes. An advantage of the combination of the two measurement principles is their suitability for the detection of surface changes with different severity.

- Grinding burn limit in the P_c''-Δt-diagram for visible tempering zones
- BN analysis for beginning (residual stress) changes

Furthermore, the BN limit value can be individually adjusted to allow changes of the surface state up to a defined point. The applicability was demonstrated for a cylindrical and a non-circular grinding process. Thereby, special attention was paid to the following points and results.

- Use of the grinding power measured at the spindle (instead of calculating P_c'' from the tangential force) is possible with an individual correction function
- Contact conditions during non-circular grinding of cams affect the exposition to thermal impact as well as the contact of the BN sensor and require consideration of some points
- Application of the process model with location-dependent calculation of P_c'' and Δt
- Using the ratio of BN of a ground and a reference surface
- Grinding of workpieces with low mass leads to a mechanical influenced BN signal which can be eliminated using a Short-Time Fourier Transformation

Finally, a concept for a grinding process control was suggested.

- Closed-loop control based on a soft sensor combining P_C'' and BN
- Controlled variable: surface state
- Manipulated variable: radial feed speed v_{fr} or dressing interval

It promises maximum productivity while excluding thermo-mechanical damages due to optimization of the radial feed speed respectively the dressing interval. However, further validation is required for use in practice.

Acknowledgements The scientific work has been supported by the German Research Foundation (DFG) within the research priority program SPP 2086 for project KA1006/28-2, EP128/3-2 and DI2165/5-2 project number 401804277. The authors thank the DFG for this funding and intensive technical support.

Author contributions Conceptualization: RJ; Formal analysis and investigation: RJ, GK (cylindrical grinding) and MR (non-circular grinding); Writing—original draft preparation: RJ, GK and MR; Writing—review and editing: MD, JE and BK; Supervision and project administration: MD, JE and BK. All authors read and approved the final manuscript.

Funding Open Access funding enabled and organized by Projekt DEAL.

Declarations

Conflict of interest The authors declare that they have no conflict of interest.

Open Access This article is licensed under a Creative Commons Attribution 4.0 International License, which permits use, sharing, adaptation, distribution and reproduction in any medium or format, as long as you give appropriate credit to the original author(s) and the source, provide a link to the Creative Commons licence, and indicate if changes were made. The images or other third party material in this article are included in the article's Creative Commons licence, unless indicated otherwise in a credit line to the material. If material is not included in the article's Creative Commons licence and your intended use is not permitted by statutory regulation or exceeds the permitted use, you will need to obtain permission directly from the copyright holder. To view a copy of this licence, visit http://creativecommons.org/licenses/by/4.0/.

References

1. Altpeter I, Boller C, Kopp M, et al. (2011) Zerstörungsfreie Detektion von Schleifbrand mittels elektromagnetischer Prüftechniken. DGZfP-Jahrestagung 2011, Bremen

2. Karpuschewski B, Bleicher O, Beutner M (2011) Surface Integrity Inspection on Gears Using Barkhausen Noise Analysis. Procedia Eng 19:162–171. https://doi.org/10.1016/j.proeng.2011.11.096
3. Theiner WA (1997) Micromagnetic techniques. In: Hauk V (ed) Structural and Residual Stress Analysis by Nondestructive Methods. Elsevier Science B.V, Amsterdam, pp 564–589
4. Barkhausen HG (1919) Zwei mit Hilfe der neuen Verstärker entdeckte Erscheinungen. Phys Z 20:401
5. Buttle D J (2013) Magnetic Methods. In: Schajer G S (ed) Practical Residual Stress Measurement Methods. Wiley-Verlag, pp. 225–258
6. Thiemann P, Ströbel G (2013) Mikromagnetische und photothermische Charakterisierung thermo-mechanischer Schädigungen. TM Tech Mess 80(6):206–212. https://doi.org/10.1524/teme.2013.0020
7. Sackmann D, Karpuschewski B, Epp J et al (2019) Detection of surface damages in ground spur gears by non-destructive micromagnetic methods. Forsch Ingenieurwes 83(3):563–570. https://doi.org/10.1007/s10010-019-00368-z
8. Heinzel J, Jedamski R, Rößler M et al (2022) Hybrid approach to evaluate surface integrity based on grinding power and Barkhausen noise. Procedia CIRP 108:489–494. https://doi.org/10.1016/j.procir.2022.03.076
9. Tönshoff HK, Karpuschewski B, Regent C (1999) Process monitoring in grinding using micromagnetic techniques. Int J Adv Manuf Tech 15(10):694–698. https://doi.org/10.1007/s001700050121
10. Karpuschewski B (2001) Sensors for Physical Properties. In: Tönshoff HK, Inasaki I (eds) Sensors for Manufacturing. Wiley, pp 123–142
11. Pierer A, Gentzen J (2018) Möglichkeiten zur In-Prozess-Bewertung von thermischen Randzonenschädigungen beim Schleifen. In: Hoffmeister H-W, Denkena B (ed) Jahrbuch Schleifen, Honen, Läppen und Polieren, Verfahren und Maschinen. Vulkan Verlag, pp.
12. Jedamski R, Heinzel J, Rößler M et al (2020) Potential of magnetic Barkhausen noise analysis for in-process monitoring of surface layer properties of steel components in grinding. TM Tech Mess 87(12):787–798. https://doi.org/10.1515/teme-2020-0048
13. Rößler M, Dix M, Heinzel J et al (2022) Überwachung der Randzone beim Unrundschleifen. WT Werkstattstech 112(11–12):745–748
14. Malkin S, Guo C (2007) Thermal Analysis of Grinding. CIRP Ann 56(2):760–782. https://doi.org/10.1016/j.cirp.2007.10.005
15. Brinksmeier E, Aurich JC, Govekar E et al (2006) Advances in Modeling and Simulation of Grinding Processes. CIRP Ann 55(2):667–696. https://doi.org/10.1016/j.cirp.2006.10.003
16. Jermolajev S, Brinksmeier E (2014) A new approach for the prediction of surface and subsurface properties after grinding. Advanced Materials Research 1018:189–196. https://doi.org/10.4028/www.scientific.net/AMR.1018.189
17. Heinzel C, Heinzel J, Guba N et al (2021) Comprehensive analysis of the thermal impact and its depth effect in grinding. CIRP Ann 70(1):289–292. https://doi.org/10.1016/j.cirp.2021.04.010
18. Guba N, Heinzel J, Heinzel C et al (2020) Grinding burn limits: Generation of surface layer modification charts for discontinuous profile grinding with analogy trials. CIRP J Manuf Sci Technol 31:99–107. https://doi.org/10.1016/j.cirpj.2020.09.014
19. Malkin S, Lenz E (1978) Burning limit for surface and cylindrical grinding of steels. CIRP Ann 27(1):233–236
20. Heinzel J (2022) Thermische Prozessgrenzen beim Schleifen erkennen. Dissertation, Universität Bremen
21. Stampfer B, González G, Gerstenmeyer M, et al. (2021) The Present State of Surface Conditioning in Cutting and Grinding. J. Manuf. Mater. Process. 5(3). https:// https://doi.org/10.3390/jmmp5030092
22. Schulze V, Zanger F, Stampfer B et al (2020) Surface conditioning in machining processes. TM Tech Mess 87(11):661–673. https://doi.org/10.1515/teme-2020-0044
23. Lin B, Recke B, Knudsen JKH et al (2007) A systematic approach for soft sensor development. Comput Chem Eng 31(5–6):419–425. https://doi.org/10.1016/j.compchemeng.2006.05.030
24. Klocke F (2017) Fertigungsverfahren 2. Springer Vieweg, Berlin, Heidelberg
25. Heinzel C, Kirsch B, Meyer D et al (2020) Interactions of grinding tool and supplied fluid. CIRP Ann 69(2):624–645. https://doi.org/10.1016/j.cirp.2020.05.001
26. Jedamski R, Heinzel J, Karpuschewski B, et al. (2022) In-Process Measurement of Barkhausen Noise for Detection of Surface Integrity during Grinding. Appl. Sci. 12(9)
27. Denkena B, Tönshoff HK (2011) Spanen—Grundlagen, 3rd edn. Springer-Verlag, Berlin—Heidelberg
28. Spieß L, Teichert G, Robert S, et al. (2019) Moderne Röntgenbeugung. Röntgendiffraktometrie für Materialwissenschaftler, Physiker und Chemiker. Springer Spektrum, Wiesbaden
29. Jedamski R, Gerhardt B, Müller C, et al. (2023) Detektierbarkeit thermomechanischer Randzonenschädigungen an Vergütungs-, Nitrier- und Einsatzstählen mittels Barkhausenrauschanalyse. HTM—J. Heat Treat. Mater. 78(1): 32–48. https://doi.org/10.3390/jmmp503009210.1515/htm-2022-1036
30. Rößler M, Putz M, Hochmuth C et al (2021) In-process evaluation of the grinding process using a new Barkhausen noise method. Procedia CIRP 99:202–207. https://doi.org/10.1016/j.procir.2021.03.028
31. Heinzel J, Jedamski R, Epp J et al (2021) In-process measurement of Barkhausen noise and resulting productivity increase potential in grinding of case hardened steel. CIRP J Manuf Sci Technol 32:37–45. https://doi.org/10.1016/j.cirpj.2020.11.011
32. Hochmuth C (2017) Industrie 4.0—Entwicklung adaptiver Beabeitungsprozesse. Fachseminar Feinbearbeitung, Chemnitz

Publisher's Note Springer Nature remains neutral with regard to jurisdictional claims in published maps and institutional affiliations.